Development of ATX and DUSP inhibitors : inhibiting phosphate ester hydrolysis in biology

Albers, H.M.H.G.

CHAPTER 3

Discovery and optimization of boronic acid-based inhibitors of autotaxin: *How did we exactly arrive at these inhibitors?*

Harald M.H.G. Albers, Laurens A. van Meeteren, David A. Egan, Erica W. van Tilburg, Wouter H. Moolenaar and Huib Ovaa, *Journal of Medicinal Chemistry* **2010**, *53*, 4958-4967.

Abstract. Autotaxin (ATX) is an extracellular enzyme that hydrolyzes lysophosphatidylcholine (LPC) to produce the lipid mediator lysophosphatidic acid (LPA). The ATX-LPA signaling axis has been implicated in diverse physiological and pathological processes, including vascular development, inflammation, fibrotic disease and tumor progression. Therefore, targeting ATX with small molecule inhibitors is an attractive therapeutic strategy. The previous chapter describes thiazolidine-2,4-diones that inhibit ATX activity in the micromolar range. Interestingly, inhibitory potency was dramatically increased by introduction of a boronic acid moiety, designed to target the active site threonine in ATX. Here the discovery and further optimization of boronic acid-based ATX inhibitors is described. The most potent of these compounds inhibits ATX-mediated LPC hydrolysis in the nanomolar range (IC_{50} = 6 nM). The finding that ATX can be targeted by boronic acids may aid the development of ATX inhibitors for therapeutic use.

3.1 Introduction

Autotaxin (ATX or ENPP2), originally isolated as an autocrine motility factor from melanoma cells, belongs to the ecto-nucleotide pyrophosphatase and phosphodiesterase (ENPP) family.[1-3] This extracellular enzyme acts as a lysophospholipase D, hydrolyzing lysophosphatidylcholine (LPC) into the lipid mediator lysophosphatidic acid (LPA), as depicted in Scheme 1.[4,5] Hydrolytic activity of ATX originates from a threonine (T210) residue in the active site.[1] LPA activates specific G protein-coupled receptors and thereby stimulates the migration, proliferation and survival of many cell types.[6]

The ATX-LPA axis has a vital role in vascular development.[7,8] Furthermore, it has been implicated in various pathologies including tumor progression[9] and metastasis,[10] inflammation[11] and fibrotic disease.[12] Given its role in human disease, the ATX-LPA axis is an obvious target for therapy. The fact that ATX is an extracellular enzyme makes it even more attractive as a drug target. Since there are at least six distinct LPA receptors, direct targeting of LPA receptors seems to be a less attractive strategy.[13,14] On the basis of the initial discovery that ATX is inhibited by LPA and sphingosine 1-phosphate (S1P) under certain conditions,[15] various synthetic phospholipid analogs have been explored as ATX inhibitors.[16-20] However, lipid-based inhibitors have the disadvantage that they could act as agonists or antagonists for any of the LPA/S1P receptors, thereby resulting in an effect opposite of the one intended. In addition, non-lipid ATX inhibitors have been identified, but their inhibitory potential is low (IC_{50} ≥ 1 μM).[21-23]

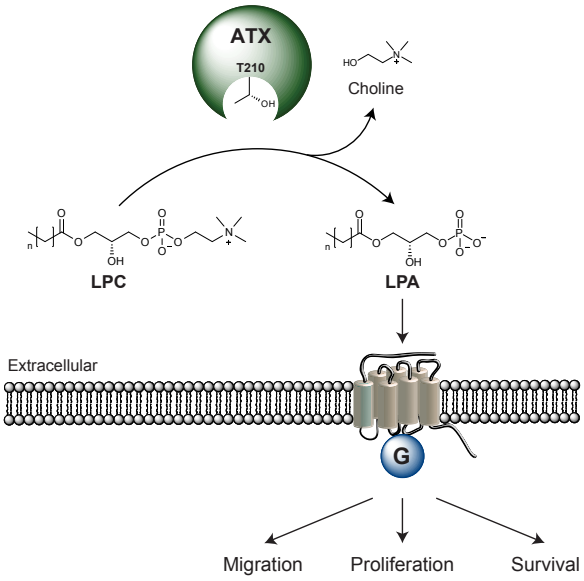

Scheme 1. The hydrolysis of LPC by ATX into LPA and choline. The lysoPLD reaction is catalyzed by a threonine oxygen nucleophile (T210). Newly produced LPA triggers subsequent biological events *via* activation of specific G protein-coupled receptors.

The previous chapter describes a non-lipid ATX inhibitor (HA130)[24] that rapidly lowers plasma LPA levels upon intravenous injection in mice. Using HA130 we found that the turnover of circulating LPA is much faster than expected, showing the usefulness of ATX inhibitors as tools to elucidate the role of ATX and LPA *in vivo*.

Here we describe the discovery and optimization of boronic acid-based inhibitors of ATX. We screened ~40,000 small molecules and identified thiazolidine-2,4-dione as ATX

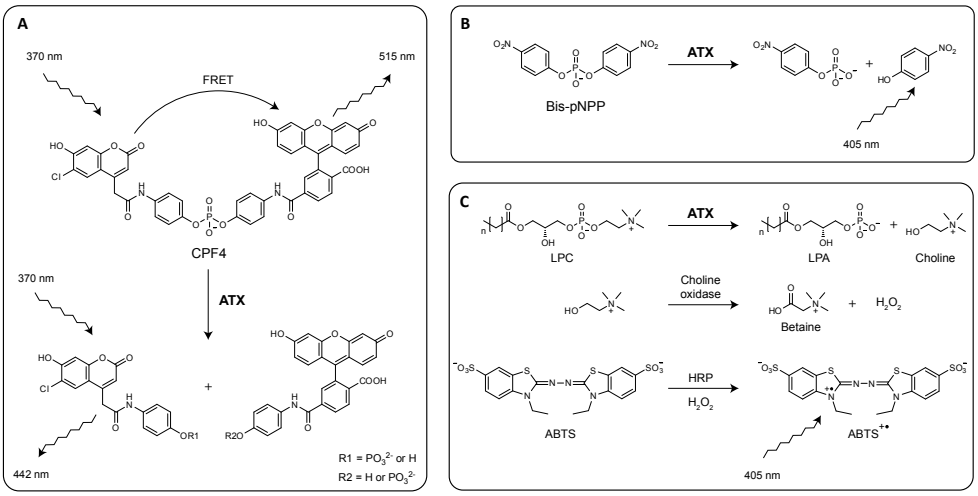

Figure 1. Three ATX assays used for screening and validation of ATX inhibitors. (A) CPF4 assay; This assay is based on Förster resonance energy transfer (FRET) between coumarin and fluorescein moieties of CPF4. (B) Bis-pNPP assay; In this assay bis-*para*-nitrophenyl phosphate (bis-pNPP) is hydrolyzed by ATX into the chromophore *para*-nitrophenol. (C) Choline release assay; The physiological substrate of ATX, LPC, is hydrolyzed by ATX to give LPA and choline. The release of choline can be detected in a two-step enzymatic coloring reaction.

inhibitors, which proved to be suitable to further chemical optimization. In particular, we optimized these molecules by first introducing small systematic variations in the structure of a screening hit, followed by the introduction of more random variations. Finally, by targeting the T210 oxygen nucleophile in ATX through a boronic acid, the potency of the original thiazolidine-2,4-dione screening hit was increased over 400-fold (IC_{50} = 6 nM).

3.2 ATX inhibitor screen

To identify ATX inhibitors, a small molecule screen was carried out. We first used a collection of 17,500 molecules from the National Cancer Institute (NCI) to optimize our screening protocol. This NCI library was initially screened using CPF4, an ATX activity reporter based on Förster resonance energy transfer (FRET) (Figure 1A).[15,25] The phosphodiester bond which links the coumarin and fluorescein moieties in CPF4 is hydrolyzed by ATX, resulting in the loss of FRET. Since we have shown that LPA can inhibit ATX activity in this assay, it was used as a positive control for ATX inhibition.[15] Approximately 250 active molecules were retested in a second assay using bis-*para*-nitrophenyl phosphate (bis-pNPP) as reporter substrate (Figure 1B).[15] In Supporting Figure S1 the results of both assays are compared. Only a few compounds remained after retesting in the bis-pNPP assay. Since the CPF4 assay resulted in many false positives, we decided to reverse the assay order. The same NCI library was tested in the bis-pNPP assay using CPF4 as confirmation tool which led to reproducible hits corresponding to the findings of Saunders *et al*.[26] Top three actives of the NCI screen can be found in Supporting Figure S2.

Structure	Entry	PI (%)		IC_{50} (nM)
		Bis-pNPP	*CPF4*	*Bis-pNPP*
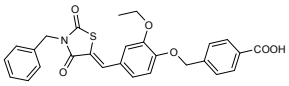	**1**	92	89	161
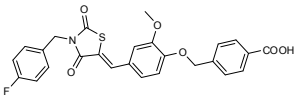	**2** (**A**)	91	85	56
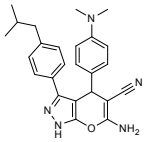	**3**	87	77	46
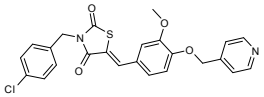	**4**	83	85	68
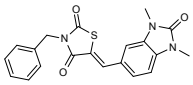	**5**	75	55	111
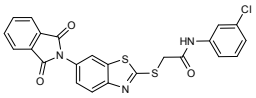	**6**	71	66	261
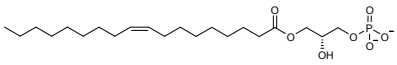	LPA	80	67	442

Figure 2. ATX inhibitors discovered by high-throughput screening. Percentage inhibition (PI) at 5 µM is based on the bis-pNPP or CPF4 assay. IC_{50} values are obtained using the bis-pNPP assay. LPA was used as a control for ATX inhibition.

After setting up our screening protocol, we used a commercial library (SPECS) consisting of 23,000 small molecules with predicted drug-like properties. For active molecules in this screen the percentage inhibition (PI) at 5 µM and IC_{50} values (bis-pNPP assay) are shown in Figure 2. These actives were confirmed by the CPF4 assay (Figure 2). Among the confirmed active molecules were several thiazolidine-2,4-diones (**1**, **2**, **4** and **5**), a pyrano pyrazole (**3**) and a benzothiazole (**6**). Because the thiazolidine-2,4-diones are well represented among the positive hits and their amenability to fast chemical diversification, the most potent thiazolidine-2,4-dione **2** (IC_{50} = 56 nM) was selected for further optimization.

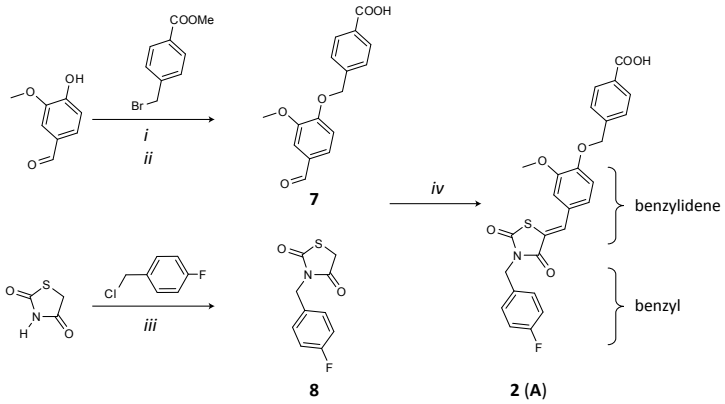

Scheme 2. Convergent synthetic route towards thiazolidine-2,4-dione **2** (**A**). *Reagents (i) KOH, DMSO, rt, 30 min. (ii) NaOH, DMSO/H_2O (1:3, v/v), reflux, 4 h, 91%. (iii) NaH, DMF, rt, 22 h, 74%. (iv) Piperidine, EtOH, reflux, 20 h, 63%.*

3.3 Chemistry

We next explored how to improve the potency of thiazolidine-2,4-dione **2** (compound **A** in Chapter 2) as an ATX inhibitor. We designed the convergent synthetic route toward inhibitor **2** depicted in Scheme 2. The synthesis requires benzoic acid **7** which can be obtained *via* a one-pot-synthesis. First, vanillin was *O*-alkylated with methyl-4-(bromomethyl) benzoate.[27] The resulting benzoate was hydrolyzed to give benzoic acid **7**. To afford the precursor **8**, thiazolidine-2,4-dione was dissolved in DMF and *N*-alkylated with 4-fluorobenzyl chloride in the presence of sodium hydride. Finally, monosubstituted thiazolane-2,4-dione **8** was reacted *via* a Knoevenagel condensation with benzoic acid **7**.[28] *Z*-isomer **2** precipitated during reaction and washing the precipitate with ethanol resulted in homogeneous product (For ^{1}H NMR and HPLC spectra see Supporting Figure S3). The synthetic route toward **2** appeared to be applicable for the fast parallel synthesis and purification of many analogs without the need for chromatography.

3.4 Systematic optimization

Inhibitor **2** contains two side chains attached to the thiazolidine-2,4-dione core, a benzyl and a benzylidene moiety (Scheme 2). To explore structure-activity relationships (SAR), we first generated a small library before embarking on a bigger effort. This resulted in the molecules listed in Table 1. LPA was used as a control that it inhibits the ATX-mediated hydrolysis of bis-pNPP by ATX (IC_{50} = 0.4 μM).[15]

The best series of inhibitors are the benzoic acids (**2** and **9**-**11**), where the fluorinated compound **2** has the highest activity (IC_{50} = 56 nM) in the bis-pNPP assay (Table 1). Replacement of the 4-fluorine atom (**2**) for hydrogen (**9**), nitro- (**10**) or a *tert*-butyl group (**11**) reduced the potency of the inhibitor with increasing size of the functional group. With the replacement of the carboxylic acid in molecules **2** and **9**-**11** by a methyl ester (**12**-**15**), potency

Table 1. Structure-activity data for molecules of the systematic optimization. IC_{50} values and residual ATX activity (RA) of the synthesized thiazolidine-2,4-dione derivatives using the artificial ATX substrate bis-pNPP (na: not active at 5 μM).

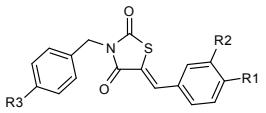

R1	R2	R3	Entry	IC_{50} (μM)	RA (%)
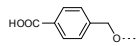	OMe	H	**9**	0.248	9
	OMe	F	**2**	0.056	10
	OMe	NO_2	**10**	0.442	33
	OMe	$C(CH_3)_3$	**11**	18.2	33
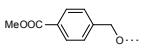	OMe	H	**12**	2.69	24
	OMe	F	**13**	>100	-
	OMe	NO_2	**14**	60.9	31
	OMe	$C(CH_3)_3$	**15**	>100	-
	OMe	H	**16**	>100	-
	OMe	F	**17**	5.87	12
	OMe	NO_2	**18**	>100	-
	OMe	$C(CH_3)_3$	**19**	na	-
	H	H	**20**	2.69	32
	H	F	**21**	0.700	37
	H	NO_2	**22**	>100	-
	H	$C(CH_3)_3$	**23**	>100	-
H	H	H	**24**	>100	-
	H	F	**25**	>100	-
	H	NO_2	**26**	na	-
	H	$C(CH_3)_3$	**27**	na	-
-	-	-	LPA	0.442	39

is largely lost. Omitting the carboxylic acid (**16**-**19**) has the same effect. With removal of the methoxy group (R2) in molecules **16**-**19**, activity is regained (compare **16-19** with **20-23**). SAR analysis showed that the optimal combination of groups would be R1 = -OCH_2-Ph-COOH, R2 = H and R3 = F.

Encouraged by the SAR results suggesting that the methoxy and carboxylic acid groups are important moieties, molecules **28**-**30** were synthesized (Figure 3A). Molecules **2**, **9**-**11** and **28**-**30** were validated in the physiologically more relevant LPC hydrolysis (choline release) assay.[17] The ATX-mediated release of choline from LPC is detected by a two-step enzymatic colorimetric reaction (Figure 1C). In the first step choline is oxidized by choline oxidase into betaine (trimethylglycine) and hydrogen peroxide. Horseradish peroxidase (HRP) then consumes hydrogenperoxide to oxidize 2,2'-azino-bis(3-ethylbenzothiazoline-6-sulfonic acid) (ABTS) to a radical cation species which absorbs at 405 nm.

The data obtained from the choline release assay are summarized in Figure 3A. The IC_{50} values obtained were some 10-fold higher than observed in with bis-pNPP as a substrate. It is noteworthy that compound **10** is incapable of fully inhibiting ATX at high concentrations (Figure 3B). This residual ATX activity for **10** is about 60%. However, **10** shows inhibition at a lower concentration than **11** which was also observed in the bis-pNPP assay. LPA did not inhibit ATX in the choline release assay as observed by Ferry *et al*.[19]

The established SAR was confirmed by the more active molecule **28** (IC_{50} = 1.63 μM) in which the methoxy group in **2** (IC_{50} = 2.50 μM) is omitted. Changing the carboxylic acid of **2** from *para* to the *meta* position results in the more potent inhibitor **29** (IC_{50} = 2.05 μM) but less potent than **28**. Changing the carboxylic acid in **28** from *para* to *meta* (**30** (HA51), IC_{50} = 1.07 μM) results in the most active molecule in this systematic optimization with a 2.5-fold reduction in IC_{50} value compared to **2** and also to a further reduction in residual ATX activity (from 35 to 7%) in the choline release assay.

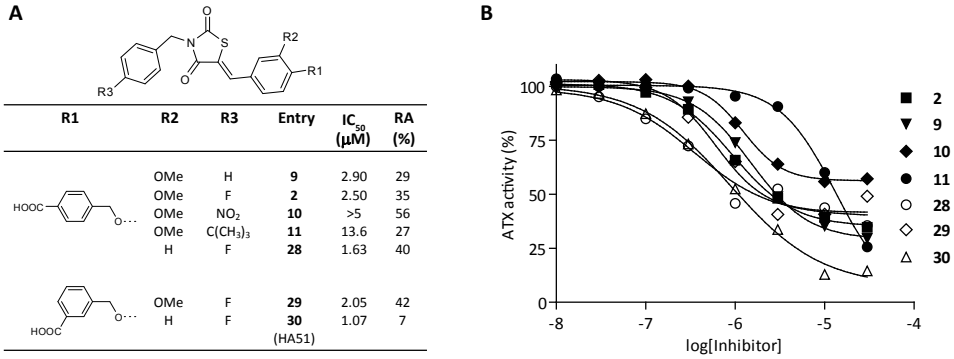

Figure 3. Validation of screening hit **2** and the benzoic acids of the systematic optimization in the choline release assay. (A) Structure-activity data of the systematic optimization. Residual ATX activity is abbreviated by RA (%). (B) Dose-response curves for the benzoic acids.

3.5 Variation in the benzyl moiety

Since our initial systematic optimization of **2** provided good structure-activity correlations we varied either the benzyl or the benzylidene moiety (Scheme 2). In this approach, either the benzyl or the benzylidene moiety corresponds to the screening hit **2** while the other part is alternated. First, the effect of changes in the benzyl part of the molecule was investigated by introducing halogens. The percentage inhibition (PI) values at 5 μM of compounds **31**-**40**, as measured by the choline release assay, are listed in Table 2. The most potent inhibitor was bromo compound **39** (PI = 73%). However, its IC_{50} (2.80 μM) is similar to that of screening hit **2** (IC_{50} = 2.50 μM). Other substituents (**41**-**71**) that were explored did not result in significant improvements.

3.6 Variation in the benzylidene moiety.

Next, variations were incorporated into the benzylidene moiety, resulting in molecules shown in Supporting Table S1. In contrast to the variation in the benzyl moiety, few molecules were active; only 30% of the compounds tested showed inhibition (PI_{max} = 12%). This indicates that variations in the benzylidene moiety of screening hit **2** are not well tolerated.

3.7 Boronic acid introduction and optimization

Because the benzyl and benzylidene moiety variations did not improve inhibition, we modified inhibitor **30** that resulted from the systematic optimization. Replacing the carboxylic acid in molecule **30** by a boronic acid resulted in molecule **72** (HA130, Table 3). We recently characterized **72** as a potent ATX inhibitor both *in vitro* and *in vivo*.[24] We reasoned that the carboxylic acid moiety in molecule **30** could act as a phosphate mimic that binds near or at the active site threonine (T210). Replacing the carboxylic acid in molecule **30** by a boronic

Table 2. Derivatives of screening hit **2** with a structural variation in the benzyl moiety (R). Percentage inhibition (PI, %) has been determined in the choline release assay at 5 µM. Molecules that show more than 50% inhibition are in bold (**compound** / PI).

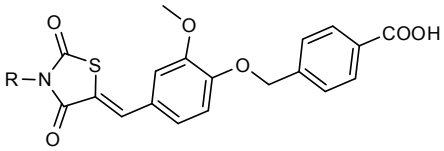

					
2 / 55%	**31** / 64%	**32** / 41%	**33** / 57%	**34** / 29%	**35** / 57%
					
36 / 38%	**37** / 23%	**38** / 26%	**39** / 72%	**40** / 51%	**41** / 21%
					
42 / 44%	**43** / 17%	**44** / 48%	**45** / 38%	**46** / 13%	**47** / 17%
					
48 / 10%	**49** / 32%	**50** / 46%	**51** / 28%	**52** / 13%	**53** / 12%
					
54 / 10%	**55** / 11%	**56** / 20%	**57** / 35%	**58** / 23%	**59** / 17%
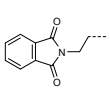					
60 / 0%	**61** / 4%	**62** / 13%	**63** / 11%	**64** / 5%	**65** / 19%
					
66 / 15%	**67** / 31%	**68** / 49%	**69** / 42%	**70** / 31%	**71** / 30%

acid could well be a good ATX targeting strategy. This strategy was inspired by the proteasome inhibitor bortezomib, which targets the N-terminal threonine oxygen nucleophile in the proteasome through a boronic acid.[29] Furthermore, boronic acids have been reported to inhibit β-lactamases through targeting of the active site serine residue.[30]

The boronic acid modification resulted in a 100-fold more potent inhibitor (IC_{50} = 28 nM) compared to screening hit **2** (IC_{50} = 2.50 µM). When the position of the boronic acid was changed from *meta* (**72**) to the *para* (**73**) position, potency increased by another 5-fold (IC_{50} = 5.7 nM), while the potency of the *ortho* boronic acid **74** dropped (IC_{50} > 5.00 µM). Next, the

Table 3. Potent ATX inhibitors of the boronic acid optimization. For the boronic acids percentage inhibition (PI, %) at 5 μM and IC_{50} values have been determined in the choline release assay (PI / IC_{50}).

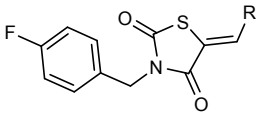

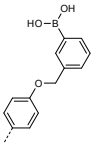	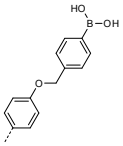	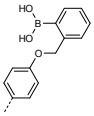	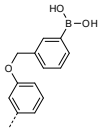	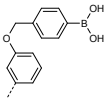	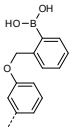
72 (HA130)	**73** (HA155)	**74**	**75**	**76**	**77**
99% / 28.3 nM	99% / 5.67 nM	36% / >5.00 μM	100% / 11.9 nM	100% / 29.6 nM	11% / >5.00 μM

3-benzyloxy boronic acids analogs **75**-**77** were synthesized. The *meta* boronic acid (**75**) proved to be more potent than the *para* (**76**) and the *ortho* boronic acid (**77**) has a low potency.

3.8 Effect inhibitors on readout choline release assay

An inherent danger of the choline release assay is that small molecules can interfere with the readout by inhibiting the enzymes (horseradish peroxidase or choline oxidase) used in the coloring reaction, resulting in false positives. Another way to interfere with the choline release assay is that compounds can react with the ABTS or hydrogen peroxide generated during the coloring reaction. The latter could be an issue for the boronic acids reported here because aliphatic and aryl boronic acids have the ability to react with hydrogen peroxide.[31-33] We investigated the effect of the inhibitors **72**, **73**, **75** and **76** on the coloring reaction, and no effect was observed (Supporting Figure S4). Therefore, the choline release assay is a valid way to test the synthesized compounds here on ATX inhibition.

3.9 Mode of inhibition

For inhibitors **2**, **30**, **72** and **73**, the mode of inhibition was determined from a Lineweaver-Burk plot (Supporting Figure S5). Inhibitors **2** and **30** inhibit in a competitive manner using LPC as substrate. Kinetic analysis for boronic acids **72** and **73** revealed a mixed type inhibition.

Because these inhibitors contain a Michael acceptor, it could be that these inhibitors react irreversibly with ATX (or other enzymes), which is undesirable. When ATX is incubated with 5 μM inhibitor **2**, **30**, **72** or **73** for 20 min at 310 K and these solutions are then washed with ethyl acetate, ATX activity is restored up to 97% of its original activity in the choline release assay (Supporting Figure S6). This indicates that these inhibitors reversible bind to ATX.

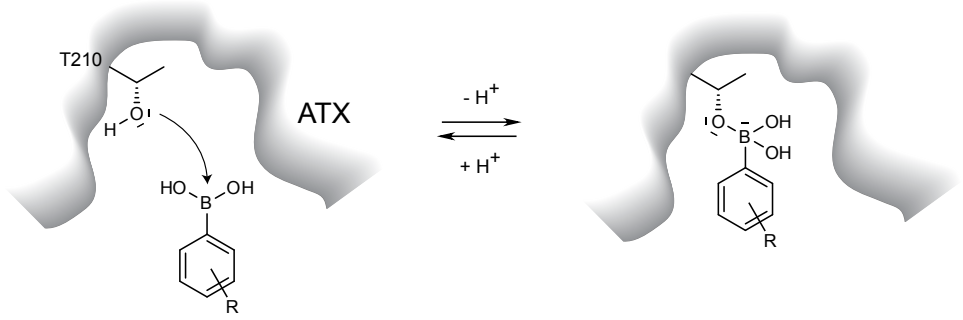

Figure 4. Our hypothesis on the binding of boronic acid-based ATX inhibitors with the T210 oxygen nucleophile in the ATX active site.

3.10 Discussion and conclusions

This study shows that ATX can be targeted efficiently by boronic acid inhibitors. We discovered thiazolidine-2,4-diones as potent non-lipid ATX inhibitors. Replacing the carboxylic acid by a boronic acid in thiazolidine-2,4-dione screening hit **2** resulted in a 440-fold more active inhibitor (IC_{50} = 2.50 µM → 6 nM).

We handed three different approaches for optimization of screening hit **2**. The first is the systematic optimization of **2**, which led to a 2.5-fold increase in potency in the choline release assay. The second is a randomized approach, changing separately the benzyl and the benzylidene parts of the molecule. This did not result in significantly more potent molecules. Finally, we replaced the carboxylic acid in screening hit **2** by a boronic acid. Our rationale was that the carboxylic acid could function as a phosphate mimic and thereby bind near or at the T210 oxygen nucleophile. In that case, the T210 oxygen nucleophile in ATX can be targeted *via* a boronic acid. A similar strategy has proven successful for the proteasome inhibitor bortezomib which binds to threonine oxygen nucleophile in the proteasome active site through the boronic acid moiety.[29] Replacing the carboxylic acid moiety in screening hit **2** (IC_{50} = 2.50 µM) by a boronic acid resulted in molecule **73** (IC_{50} = 6 nM), which is over 400-fold more potent than inhibitor **2**. These results demonstrate that ATX activity can be targeted by boronic acids. Next, to their increased affinity for ATX, the boronic acids are also expected to improve selectivity over hydrolytic enzymes that depend on a sulfur (cysteine) nucleophile, as is commonly found in phosphate ester hydrolyzing enzymes.

Kinetic analysis showed that inhibitors **2** and **30** inhibit in a competitive manner indicating that they bind at the active site of ATX. The acid moiety of these inhibitors likely mimics the phosphate group, facilitating inhibition. Boronic acids **72** and **73** show a mixed-type inhibition. It is expected that the boronic acids have the same binding site as their carboxylic acid equivalents **2** and **30** based on their structural similarity. Binding of the boronic acid to the T210 oxygen nucleophile likely results in the Lineweaver-Burk plot

observed. The washout experiment reveals that inhibitors **2**, **30**, **72** and **73** all bind to ATX in a reversible manner. Figure 4 shows how the boronic acid inhibitors may bind to the T210 oxygen nucleophile of ATX.

In summary, we have identified thiazolidine-2,4-diones as ATX inhibitors and have found that targeting ATX with a boronic acid moiety resulted in a >400-fold increase in potency. This strategy to target ATX with a boronic acid should assist the development of future ATX inhibitors.

3.11 Experimental section

Chemicals and enzymes. Small molecule libraries were obtained from the National Cancer Institute (NCI) and purchased from SPECS, Delft, the Netherlands. NCI compounds NSC101794, NSC148368 and NSC48300 are abbreviated in the text of the Supporting information by **I**, **II** and **III** respectively. SPECS compounds AN-989/40746701, AN-988/40680277, AJ-292/40674401, AN-989/41697652, AN-989/41697944 and AQ-088/4201464 are abbreviated in the text by **1**, **2**, **3**, **4**, **5** and **6** respectively. 1-Oleoyl-2-Hydroxy-*sn*-Glycero-3-Phosphocholine (LPC, 18:1) was purchased from Avanti Polar Lipids. Oleoyl-L-α-lysophosphatidic acid sodium salt (LPA, 18:1), horseradish peroxidase (HRP), choline oxidase, and all other chemicals were obtained from Sigma-Aldrich and used as received.

Recombinant ATX. See Experimental section Chapter 2.

Bis-pNPP assay.[15] ATX activity toward bis-pNPP was determined as follows. In an opaque flat-bottom 384-well plate an amount of 2 μL DMSO containing inhibitor was added to 24 μL recombinant ATX (~20 nM) in Tris-buffered saline (140 mM NaCl, 5 mM KCl, 1 mM $CaCl_2$, 1 mM $MgCl_2$ and 50 mM Tris-HCl, pH 7.8) which contained albumin from bovine serum fatty acid free (BSA-FAF) (0.2 mg ml^{-1}). Finally, 24 μL of bis-pNPP (2 mM) was added to each well and the plate was incubated for 3 h at room temperature. This mixture with DMSO alone was used as a control. For each inhibitor ten concentrations were measured covering a range of 0.025 to 100 μM to determine IC_{50} values. Percentage inhibition was determined for a final concentration of 5 μM of inhibitor. Absorbance was measured in a Perkin-Elmer Envision plate reader (λ = 405 nm). The absorbance at 0 h was used to correct for molecules that absorb at 405 nm. Data were analyzed using Graphpad Prism software. IC_{50} values and percentage inhibition were determined in three independent experiments for each inhibitor. Percentage of residual activity (RA) is given as bottom value for curve fit.

CPF4 assay.[15] This assay was carried out in the same manner as the bis-pNPP assay using a substrate concentration of 2 μM. Fluorescence was monitored in a BMG Fluorstar 96-well plate reader (λ_{ex} = 355 nm, λ_{em} = 460 and 520 nm).

Choline release assay.[17] Measuring ATX activity using LPC (18:1) as substrate was determined as follows. In an opaque flat-bottom 96-wells plate (Greiner) 1 μL of DMSO containing inhibitor was added to 49 μL of recombinant ATX (~20 nM) in Tris-HCl buffer (0.01% Triton X-100 and 50 mM Tris-HCl, pH 7.4). Finally, 50 μL of 80 μM LPC (18:1) in Tris-HCl buffer (10 mM $MgCl_2$, 10 mM $CaCl_2$, 0.01% Triton X-100 and 50 mM Tris-HCl, pH 7.4) was added to each well and the plate was incubated at 310 K. The above-described mixture with DMSO alone was used as a control. LPC without ATX was taken as control for autohydrolysis of LPC. For each inhibitor ten concentrations were measured covering

a range of 0.01 to 30 μM to determine IC_{50} values. Percentage inhibition (PI) was determined for a final concentration of 5 μM of inhibitor. After 3 h of incubation, 50 μL of ABTS (2 mM) and horseradish peroxidase (5 U mL^{-1}) was added to 50 μL of the reaction mixture and absorbance was measured and used to correct for absorbance of the molecules. Finally, 50 μl choline oxidase (5 U mL^{-1}) in Tris-HCl (0.01% Triton X-100 and 50 mM Tris-HCl, pH 7.4) was added for colorimetric reaction. Absorbance was measured in a Perkin-Elmer Envision plate reader (λ = 405 nm). Data were analyzed using Graphpad Prism software.

In addition, the effect of the inhibitors on the enzymatic coloring reaction was investigated using 40 μM choline at 30 μM inhibitor using the above-described coloring reagents. No inhibition of the enzymatic reaction by inhibitors was observed.

Washout of inhibitors. ATX (~20 nM) in the same buffer used for the choline release assay was incubated with (5 μM) and without inhibitors at 310 K. After 20 min the incubation mixtures were washed out with ethyl acetate with 9 times the volume of the ATX solution. The ATX activity of these solutions was determined using the choline release assay.

Chemistry. All chemicals were obtained from Sigma-Aldrich and used without further purification. Dry *N,N*-dimethylformamide (DMF) from Biosolve was obtained by treatment with molecular molsieves (4 Å). Analytical thin layer chromatography was performed on aluminum sheets precoated with silica gel 60 F_{254}. Column chromatography was carried out on silica gel (0.035-0.070, 90 Å, Acros).

For isolation by centrifugation a Heraeus Multifuge 3 $_{S-R}$ centrifuge was used. Products were spun at 4400*g* at 277 K for 5 min. Nuclear magnetic resonance spectra (^{1}H NMR and COSY) were determined in deuterated dimethyl sulfoxide (d_6-DMSO) using a Bruker ARX 400 Spectrometer (^{1}H: 400 MHz) at 298 K, unless indicated otherwise. Peak shapes in the NMR spectra are indicated with the symbols 'd' (doublet), 'dd' (double doublet), 's' (singlet), 'bs' (broad singlet) and 'm' (multiplet). Chemical shifts (δ) are given in ppm and coupling constants *J* in Hz. DMSO (δ = 2.50 ppm) was used as internal reference.

HPLC-MS measurements were performed on a system equipped with a Waters 2795 Seperation Module (Alliance HT), Waters 2996 Photodiode Array Detector (190-750 nm), Waters Alltima C18 Column (2.1 mm x 100 mm) and an LCT™ Orthogonal Acceleration Time of Flight Mass Spectrometer. Samples were run at a flowrate of 0.40 mL min^{-1} using gradient elution (water/acetonitrile/formic acid) from 950/50/10 (*v*/*v*/*v*) to 50/950/10 (*v*/*v*/*v*). Purity of all compounds was verified by HPLC-MS. The purity of all tested compounds was determined by HPLC-MS analyses and was greater than 95%.

4-[(4-formyl-2-methoxyphenoxy)methyl]benzoic acid (7).
To a solution of vanillin (1.41 g, 9.24 mmol) and KOH (0.640 g, 11.4 mmol) in DMSO (10 mL), methyl-4-(bromomethyl)benzoate (2.00 g, 8.73 mmol) was added. The reaction mixture was stirred at room temperature and after 30 min, water (50 mL) was added and the solution was heated at 393 K for 2 h. Subsequently, 1M NaOH (aq) (10 mL) was added under relfux till solution becomes clear. Finally, the reaction mixture was poured into water and was acidified with 1 M HCl to pH 2. The precipitate was isolated by centrifugation, washed with water, and lyophilized resulting in the title compound. **Yield:** 91%. **^{1}H NMR**: δ = 12.99 (bs, 1H, OH), 9.85 (s, 1H), 7.98 (d, *J* 8.3, 2H), 7.58 (d, *J* 8.3, 2H), 7.55 (dd, *J* 1.9 and 8.3, 1H), 7.44 (d, *J* 1.8, 1H), 7.26 (d, *J* 8.3, 1H), 5.32 (s, 2H), 3.86 (s, 3H). **MS**: m/z $[M+H]^+$ calc. 287.09, obs. 287.11.

Synthesis of 3-(4-fluorobenzyl)-1,3-thiazolane-2,4-dione (8).
To a cooled solution (273 K) of thiazolidine-2,4-dione (5.87 g, 50 mmol) in DMF (100 ml) sodium hydride (60% in oil, 1.8 g, 45 mmol) was added. A solution of 1-(chloromethyl)-4-fluorobenzene (4.3

ml, 36.8 mmol) in DMF (25 ml) was added to the reaction mixture. The mixture was allowed to warm up to room temperature and was stirred for 4 h. Then the mixture was poured in ice water (250 ml) and hexane (100 ml) was added. After a night at 277 K the precipitated crystals were filtrated and dried to give a white solid. **Yield:** 74%. **^{1}H NMR**: δ = 7.34-7.14 (m, 4H), 4.65 (s, 2H), 4.26 (s, 2H). **MS**: m/z $[M+H]^+$ calc. 226.03, obs. 226.04.

Experimental details on compounds 9-30. This data is available free of charge *via* the Internet at http://pubs.acs.org.

General method for the synthesis of (2,4-dioxo-1,3-thiazolan-5-yliden) benzoic acids and benzene boronic acids.
To a solution of 1,3-thiazolane-2,4-dione **8** (0.293 mmol) in ethanol (2.5 mL), piperidine (12 μL, 0.207 mmol) and the appropriate aldehyde (0.352 mmol) were added and the solution was refluxed for 22 h. Upon cooling to room temperature the product precipitated out of solution. Centrifugation and washing with ethanol gave homogeneous compound.

4-[(4-{[3-(4-fluorobenzyl)-2,4-dioxo-1,3-thiazolan-5-yliden]methyl}-2-methoxy-phenoxy)-methyl]benzoic acid (2). Yield: 63%. COSY was used to assign chemical shifts. **^{1}H NMR**: δ = 12.99 (bs, 1H, OH), 7.97 (d, *J* 8.3, 2H), 7.92 (s, 1H), 7.56 (d, *J* 8.3, 2H), 7.38-7.16 (m, 7H), 5.27 (s, 2H), 4.82 (s, 2H), 3.84 (s, 3H). **MS**: m/z $[M-H]^-$ calc. 492.10, obs. 492.10.

3-[(4-{[3-(4-fluorobenzyl)-2,4-dioxo-1,3-thiazolan-5-yliden]methyl}phenoxy)methyl] benzene boronic acid (72). Yield: 64%. **^{1}H NMR**: δ = 8.08 (s, 2H, OH), 7.92 (s, 1H), 7.87 (s, 1H), 7.76 (d, *J* 7.4, 1H), 7.60 (d, *J* 7.1, 2H), 7.50-7.16 (m, 10H), 5.18 (s, 2H), 4.82 (s, 2H). **MS**: m/z $[M+H]^+$ calc. 464.11, obs. 464.25.

4-[(4-{[3-(4-fluorobenzyl)-2,4-dioxo-1,3-thiazolan-5-yliden]methyl}phenoxy)methyl] benzene boronic acid (73). Yield: 81%. **^{1}H NMR**: δ = 8.05 (s, 2H, OH), 7.93 (s, 1H), 7.81(d, *J* 8.0, 2H), 7.61 (d, *J* 8.9, 2H), 7.42 (d, *J* 8.3, 2H), 7.41-7.16 (m, 6H), 5.21 (s, 2H), 4.82 (s, 2H). **MS**: m/z $[M+H]^+$ calc. 464.11, obs. 464.21.

2-[(4-{[3-(4-fluorobenzyl)-2,4-dioxo-1,3-thiazolan-5-yliden]methyl}phenoxy)methyl] benzene boronic acid (74). Yield: 48%. **^{1}H NMR**: δ = 8.10 (s, 2H, OH), 7.93 (s, 1H), 7.62-7.13 (m, 12H), 5.32 (s, 2H), 4.82 (s, 2H). **MS**: m/z $[M+H]^+$ calc. 464.11, obs. 464.12.

3-[(3-{[3-(4-fluorobenzyl)-2,4-dioxo-1,3-thiazolan-5-yliden]methyl}phenoxy)methyl] benzene boronic acid (75). Yield: 40%. **^{1}H NMR**: δ = 8.10 (bs, 2H, OH), 7.94 (s, 1H), 7.87 (s, 1H), 7.76 (d, *J* 7.3, 1H), 7.51-7.16 (m, 10H), 5.16 (s, 2H), 4.82 (s, 2H). **MS**: m/z $[M+H]^+$ calc. 464.11, obs. 464.13.

4-[(3-{[3-(4-fluorobenzyl)-2,4-dioxo-1,3-thiazolan-5-yliden]methyl}phenoxy)methyl] benzene boronic acid (76). Yield: 26%. **^{1}H NMR**: δ = 8.07 (s, 2H, OH), 7.93 (s, 1H), 7.81(d, *J* 8.0, 2H), 7.49-7.16 (m, 10H), 5.19 (s, 2H), 4.82 (s, 2H). **MS**: m/z $[M+H]^+$ calc. 464.11, obs. 464.12

2-[(3-{[3-(4-fluorobenzyl)-2,4-dioxo-1,3-thiazolan-5-yliden]methyl}phenoxy)methyl] benzene boronic acid (77). Yield: 32%. **^{1}H NMR**: δ = 8.09 (s, 2H, OH), 7.94 (s, 1H), 7.57-7.12 (m, 12H), 5.29 (s, 2H), 4.83 (s, 2H). **MS**: m/z $[M+H]^+$ calc. 464.11, obs. 464.13.

3.12 References

1. Gijsbers, R. Aoki, J. Arai, H. & Bollen, M. The hydrolysis of lysophospholipids and nucleotides by autotaxin (NPP2) involves a single catalytic site. *FEBS Lett.* **538**, 60-64 (2003).
2. Clair, T. Lee, H. Y. Liotta, L. A. & Stracke, M. L. Autotaxin is an exoenzyme possessing 5'-nucleotide phosphodiesterase/ATP pyrophosphatase and ATPase activities. *J. Biol. Chem.* **272**, 996-1001 (1997).
3. Bollen, M. Gijsbers, R. Ceulemans, H. Stalmans, W. & Stefan, C. Nucleotide pyrophosphatases/ phosphodiesterases on the move. *Crit. Rev. Biochem. Mol. Biol.* **35**, 393-432 (2000).
4. Tokumura, A. et al. Identification of human plasma lysophospholipase D, a lysophosphatidic acid-producing enzyme, as autotaxin, a multifunctional phosphodiesterase. *J. Biol. Chem.* **277**, 39436-39442 (2002).
5. Umezu-Goto, M. et al. Autotaxin has lysophospholipase D activity leading to tumor cell growth and motility by lysophosphatidic acid production. *J Cell Biol* **158**, 227-233 (2002).
6. Moolenaar, W. H. van Meeteren, L. A. & Giepmans, B. N. The ins and outs of lysophosphatidic acid signaling. *BioEssays* **26**, 870-881 (2004).
7. van Meeteren, L. A. et al. Autotaxin, a secreted lysophospholipase D, is essential for blood vessel formation during development. *Mol. Cell Biol.* **26**, 5015-5022 (2006).
8. Tanaka, M. et al. Autotaxin Stabilizes Blood Vessels and Is Required for Embryonic Vasculature by Producing Lysophosphatidic Acid. *J. Biol. Chem.* **281**, 25822-25830 (2006).
9. van Meeteren, L. & Moolenaar, W. Regulation and biological activities of the autotaxin-LPA axis. *Prog. Lipid Res.* **46**, 145-160 (2007).
10. David, M. et al. Cancer cell expression of autotaxin controls bone metastasis formation in mouse through lysophosphatidic acid-dependent activation of osteoclasts. *PLoS One* **5**, e9741 (2010).
11. Kanda, H. et al. Autotaxin, an ectoenzyme that produces lysophosphatidic acid, promotes the entry of lymphocytes into secondary lymphoid organs. *Nat. Immunol.* **9**, 415-423 (2008).
12. Tager, A. et al. The lysophosphatidic acid receptor LPA1 links pulmonary fibrosis to lung injury by mediating fibroblast recruitment and vascular leak. *Nat. Med.* **14**, 45-54 (2008).
13. Meyer zu Heringdorf, D. & Jakobs, K. H. Lysophospholipid receptors: signalling, pharmacology and regulation by lysophospholipid metabolism. *Biochim. Biophys. Acta* **1768**, 923-940 (2007).
14. Murakami, M. Shiraishi, A. Tabata, K. & Fujita, N. Identification of the orphan GPCR, P2Y10 receptor as the sphingosine-1-phosphate and lysophosphatidic acid receptor. *Biochem. Biophys. Res. Commun.* **371**, 707-712 (2008).
15. van Meeteren, L. A. et al. Inhibition of autotaxin by lysophosphatidic acid and sphingosine 1-phosphate. *J. Biol. Chem.* **280**, 21155-21161 (2005).
16. Gajewiak, J. Tsukahara, R. Fujiwara, Y. Tigyi, G. & Prestwich, G. D. Synthesis, Pharmacology, and Cell Biology of sn-2-Aminooxy Analogues of Lysophosphatidic Acid. *Org. Lett.* (2008).
17. Cui, P. et al. Synthesis and biological evaluation of phosphonate derivatives as autotaxin (ATX) inhibitors. *Bioorg. Med. Chem. Lett.* **17**, 1634-1640 (2007).
18. Jiang, G. et al. α-Substituted Phosphonate Analogues of Lysophosphatidic Acid (LPA) Selectively Inhibit Production and Action of LPA. *ChemMedChem* **2**, 679-690 (2007).
19. Ferry, G. et al. S32826, A Nanomolar Inhibitor of Autotaxin: Discovery, Synthesis and Applications as a Pharmacological Tool. *J. Pharmacol. Exp. Ther.* **327**, 809-819 (2008).
20. van Meeteren, L. Brinkmann, V. Saulnier-Blache, J. Lynch, K. & Moolenaar, W. Anticancer activity

of FTY720: Phosphorylated FTY720 inhibits autotaxin, a metastasis-enhancing and angiogenic lysophospholipase D. *Cancer Lett.* **266**, 203-208 (2008).

21. Moulharat, N. Fould, B. Giganti, A. Boutin, J. & Ferry, G. Molecular pharmacology of adipocyte-secreted autotaxin. *Chem.-Biol. Interact.* **172**, 115-124 (2008).
22. Parrill, A. et al. Virtual screening approaches for the identification of non-lipid autotaxin inhibitors. *Bioorg. Med. Chem.* **16**, 1784-1795 (2008).
23. Hoeglund, A. et al. Optimization of a Pipemidic Acid Autotaxin Inhibitor. *J. Med. Chem.* **53**, 1056-1066 (2009).
24. Albers, H. M. et al. Boronic acid-based inhibitor of autotaxin reveals rapid turnover of LPA in the circulation. *Proc. Natl. Acad. Sci. USA* **107**, 7257-7262 (2010).
25. Takakusa, H. et al. Design and Synthesis of an Enzyme-Cleavable Sensor Molecule for Phosphodiesterase Activity Based on Fluorescence Resonance Energy Transfer. *J. Am. Chem. Soc.* **124**, 1653-1657 (2002).
26. Saunders, L. P. et al. Identification of small-molecule inhibitors of autotaxin that inhibit melanoma cell migration and invasion. *Mol. Cancer Ther.* **7**, 3352-3362 (2008).
27. Johnstone, R. & Rose, M. A rapid, simple, and mild procedure for alkylation of phenols, alcohols, amides and acids. *Tetrahedron* **35**, 2169-2173 (1979).
28. Bruno, G. et al. Synthesis and aldose reductase inhibitory activity of 5-arylidene-2,4-thiazolidinediones. *Bioorg. Med. Chem.* **10**, 1077-1084 (2002).
29. Groll, M. Berkers, C. Ploegh, H. & Ovaa, H. Crystal Structure of the Boronic Acid-Based Proteasome Inhibitor Bortezomib in Complex with the Yeast 20S Proteasome. *Structure* **14**, 451-456 (2006).
30. Crompton, I. E. Cuthbert, B. K. Lowe, G. & Waley, S. G. β-lactamase inhibitors. The inhibition of serine β-lactamases by specific boronic acids. *Biochem. J.* **251**, 453-459 (1988).
31. Kuivila, H. & Armour, A. Electrophilic Displacement Reactions. IX. Effects of Substituents on Rates of Reactions between Hydrogen Peroxide and Benzeneboronic Acid1-3. *J. Am. Chem. Soc.* **79**, 5659-5662 (1957).
32. Kuivila, H. Electrophilic Displacement Reactions. VI. Catalysis by Strong Acids in the Reaction between Hydrogen Peroxide and Benzeneboronic Acid1,2. *J. Am. Chem. Soc.* **77**, 4014-4016 (1955).
33. Snyder, H. R. Kuck, J. A. & Johnson, J. Organoboron Compounds, and the Study of Reaction Mechanisms. Primary Aliphatic Boronic Acids1. *J. Am. Chem. Soc.* **60**, 105-111 (1938).

3.13 Supporting information

ATX inhibitor screen NCI library

Screening a small molecule library of the National Cancer Institute (NCI) we identified xanthine and arsonate derivatives as moderate ATX inhibitors as depicted in Figure S2 using the bis-pNPP assay. Interestingly, aryl xanthines are known as phosphodiesterase 5 inhibitors.[1] The structure of arsonate **II** is related to a phenyldiazenylphenyl ATX inhibitors reported by Parrill *et al*.[2] Arsonate **III**, also known as NSC48300, was recently reported as ATX inhibitor and we also found it as screening hit.[3] However, in our hands quality control of different independent batches of arsonate **III** by HPLC-MS revealed that it contains mainly impurities while the presence of arsonate **III** could not be confirmed.

Supporting references

1. Arnold, R. et al. 8-Aryl xanthines potent inhibitors of phosphodiesterase 5. *Bioorg. Med. Chem. Lett.* **12**, 2587-2590 (2002).
2. Parrill, A. et al. Virtual screening approaches for the identification of non-lipid autotaxin inhibitors. *Bioorg. Med. Chem.* **16**, 1784-1795 (2008).
3. Saunders, L. P. et al. Identification of small-molecule inhibitors of autotaxin that inhibit melanoma cell migration and invasion. *Mol. Cancer Ther.* **7**, 3352-3362 (2008).

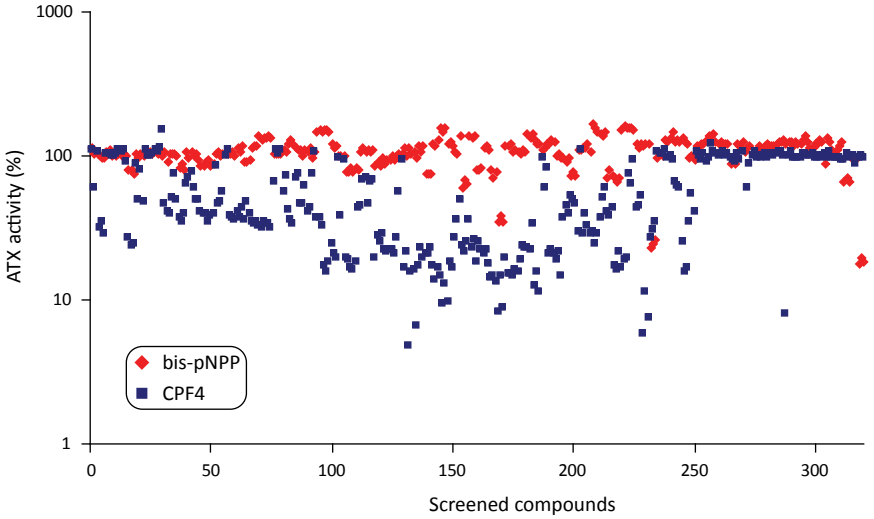

Supporting Figure S1. Primary hits obtained after screening 17,500 molecules from the NCI library using the ATX activity reporter CPF4. Bis-pNPP was used as a secondary assay to confirm the obtained hits from the initial screen. Significantly more inhibitors were identified with the CPF4 probe compared to the bis-pNPP assay. Interference with the CPF4 probe by small molecules likely leads to the many false positives observed. For this reason the bis-pNPP assay was used for further screening and the CPF4 assay for confirmation of screening hits.

Xanthine derivative **Arsonate derivatives**

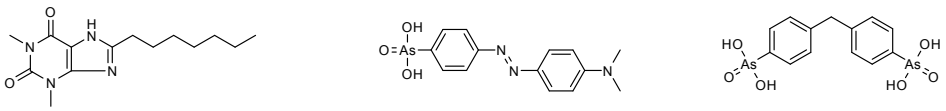

I (21%) **II** (25%) **III** (75%)

Supporting Figure S2. Structures of the identified inhibitor classes of the NCI library screen using the bis-pNPP assay. Xanthine and arsonate derivatives were identified as ATX inhibitors in the bis-pNPP assay. For each structure the percentage of ATX inhibition (PI, %) is given at an inhibitor concentration of 5 µM.

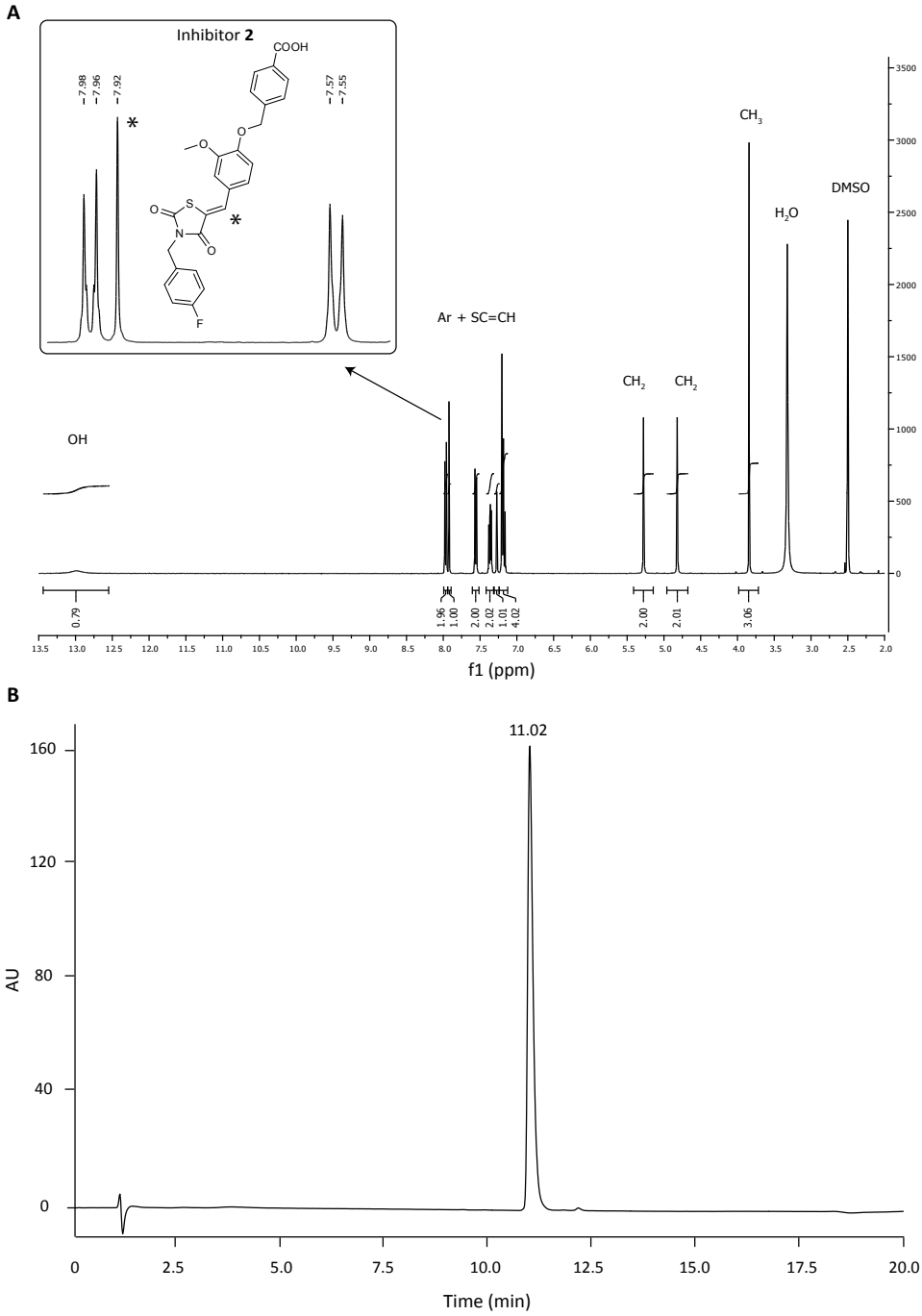

Supporting Figure S3. (A) ^{1}H NMR spectrum (d_6-DMSO) of inhibitor **2**. Inset shows the methylidene hydrogen (∗) at 7.92 ppm which is indicative for the *Z*-isomer.[28] (B) HPLC-chromatogram confirming the purity of inhibitor **2**.

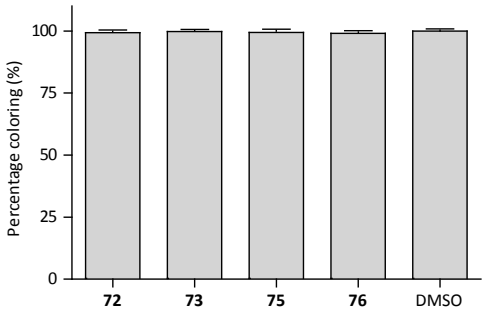

Supporting Figure S4. Effect of the active boronic acids on the readout of the choline release assay. No effect was observed on the readout using 40 µM choline at a concentration of 30 µM inhibitor.

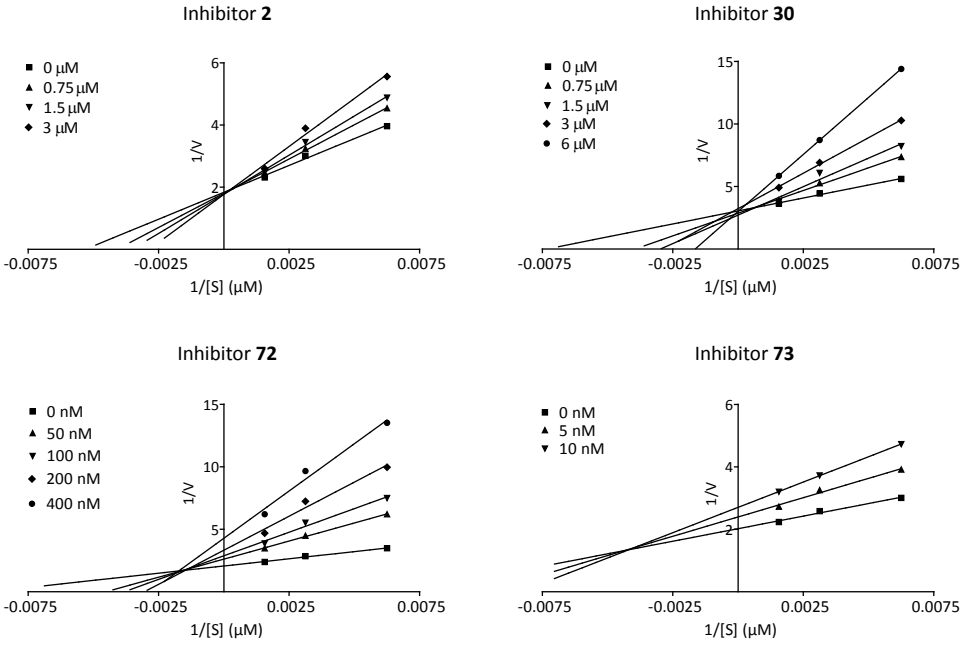

Supporting Figure S5. Lineweaver-Burk plots for the inhibitors of the optimization process. Kinetic analysis indicates competitive inhibition of ATX for **2** and **30**. Boronic acids **72** and **73** seem to inhibit in a mixed manner. Lineweaver-Burk plots were obtained from the choline release assay.

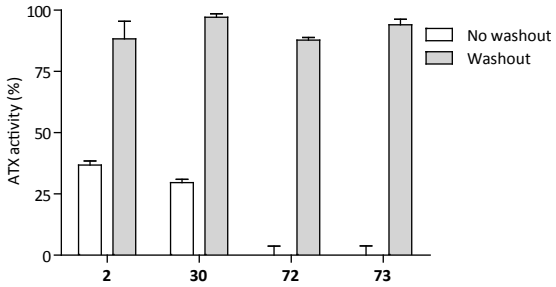

Supporting Figure S6. Washout experiment to study reversible binding the inhibitors with ATX. Incubating ATX with 5 µM of inhibitor **2**, **30**, **72** or **73** and washing out these solutions with ethyl acetate results in a recovery in ATX activity up to 97% in the choline release assay.

Supporting Table S1. Derivatives of screening hit **2** with a structural variation in the benzylidene moiety (R). Percentage inhibition (PI, %) at 5 µM has been determined in the choline release assay (**compound** / PI).

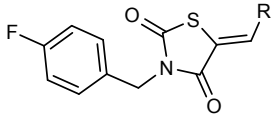

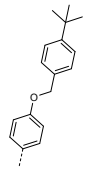 **78** / 5%	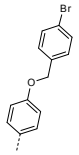 **79** / 3%	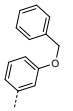 **80** / 0%	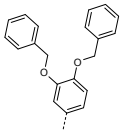 **81** / 0%	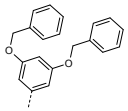 **82** / 0%	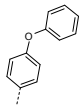 **83** / 0%
 **84** / 0%	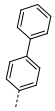 **85** / 0%	 **86** / 4%	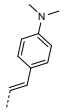 **87** / 0%	 **88** / 0%	 **89** / 0%
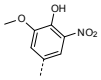 **90** / 0%	 **91** / 0%	 **92** / 0%	 **93** / 0%	 **94** / 12%	 **95** / 3%
 **96** / 4%	 **97** / 2%	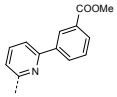 **98** / 0%	 **99** / 0%	 **100** / 0%	